

# Nanoscale

Accepted Manuscript



This is an *Accepted Manuscript*, which has been through the Royal Society of Chemistry peer review process and has been accepted for publication.

*Accepted Manuscripts* are published online shortly after acceptance, before technical editing, formatting and proof reading. Using this free service, authors can make their results available to the community, in citable form, before we publish the edited article. We will replace this *Accepted Manuscript* with the edited and formatted *Advance Article* as soon as it is available.

You can find more information about *Accepted Manuscripts* in the [Information for Authors](#).

Please note that technical editing may introduce minor changes to the text and/or graphics, which may alter content. The journal's standard [Terms & Conditions](#) and the [Ethical guidelines](#) still apply. In no event shall the Royal Society of Chemistry be held responsible for any errors or omissions in this *Accepted Manuscript* or any consequences arising from the use of any information it contains.

## N-doped graphene nanoribbons as efficient metal-free counter electrode for disulfide/thiolate redox mediated DSSCs

Yuhua Xue,<sup>a,b</sup> Janice M. Baek<sup>#,b</sup> Hao Chen,<sup>\*,a</sup> Jia Qu,<sup>\*,a</sup> Liming Dai<sup>\*,a,b</sup>

<sup>a</sup> Institute of Advanced Materials for Nano-Bio Applications, School of Ophthalmology & Optometry, Wenzhou Medical College, 270 Xueyuan Xi Road, Wenzhou, Zhejiang 325027 (China)

<sup>b</sup> Center of Advanced Science and Engineering for Carbon (Case4Carbon), Department of Macromolecular Science and Engineering, Case Western Reserve University, 10900 Euclid Avenue, Cleveland, Ohio 44106 (USA)

<sup>#</sup> On leave of absence from La Lumiere School, 6801 N. Wilhelm Rd., LaPorte, IN 46250 (USA)

\* Corresponding authors: [chenhao@mail.eye.ac.cn](mailto:chenhao@mail.eye.ac.cn); [jia.qu@163.com](mailto:jia.qu@163.com); [liming.dai@case.edu](mailto:liming.dai@case.edu)

**Abstract:** Nitrogen-doped graphene nanoribbons (N-GNRs) were prepared by thermal treatment of the as-zipped graphene oxide nanoribbon in NH<sub>3</sub> gas. X-ray photoelectron spectroscopic (XPS) measurements revealed a high nitrogen content up to 6.5 atom% for the as-prepared N-GNRs. This, together with the high Brunauer-Emmett-Teller (BET) surface area of about 751 cm<sup>2</sup>/g, prompted us to use the N-GNR as the first low-cost, metal-free counter electrode for disulfide/thiolate redox mediated dye-sensitized solar cells (DSSCs). Compared with the widely-used platinum electrode, the newly-developed N-GNR counter electrode showed a dramatically improved power conversion efficiency for DSSCs based on the thiolate/disulfide redox shuttle. The observed superior cell performance was attributed to an enhanced charge transfer capability and electrocatalytic activity induced by N-doping.

## Introduction

Dye-sensitized solar cells (DSSCs) have attracted a great deal of interest due to its high energy conversion efficiency and simple, inexpensive device fabrication.<sup>1-5</sup> A typical DSSC device consists of a photoanode, counter electrode, and electrolyte. The electrolyte, which transfers the electrons from counter electrode to photoanode electrode within the cell, plays an important role in regulating the device performance of DSSCs. The most commonly used electrolyte in DSSCs is the triiodide/iodide ( $I_3^-/I^-$ ) redox couple.<sup>1,4,5</sup> Although the triiodide/iodide couple is efficient for high-performance DSSCs, it is suffered from corrosion of silver-based current collector and partial absorption of visible light around 430 nm. Therefore, iodide-free DSSCs have been developed as an alternative choice.<sup>1,6</sup> Of particular interest, Gratzel and co-workers have developed a new electrolyte based on disulfide/thiolate ( $T_2/T^-$ ) redox couple of negligible optical absorption in the visible region, and hence potential applications in transparent DSSCs.<sup>7</sup> However, DSSCs with the disulfide/thiolate ( $T_2/T^-$ ) redox couple electrolyte often show a relatively low fill factor when platinum (Pt) is used as a counter electrode. Besides, Pt is expensive and has a limited reserve in nature. In this study, we used nitrogen-doped graphene nanoribbons (N-GNRs) as metal-free electrocatalysts to replace Pt in DSSCs with  $T_2/T^-$  electrode.

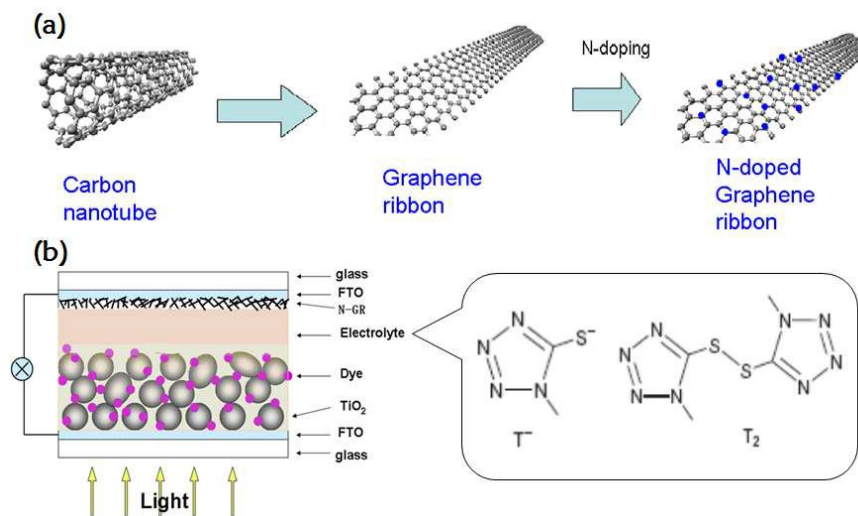
Graphene nanoribbons (GNRs) are elongated strips of graphene with straight edges, which have attracted considerable attention due to its unique structure and bandgap properties.<sup>8-12</sup> Various methods, including lithographic engineering,<sup>13,14</sup> chemical vapour deposition (CVD),<sup>15</sup> and unzipping of carbon nanotubes,<sup>8,10,11</sup> have been devised to prepare graphene nanoribbons. In the present study, we prepared N-GNRs by unzipping carbon nanotubes,<sup>8</sup> followed by thermal annealing under ammonia/argon gas mixture. Compared with pure carbon nanomaterials, the incorporation of nitrogen into carbon nanomaterials has been shown to be an effective way to

controllably turn their electronic and surface characteristics.<sup>16, 17</sup> As a result, nitrogen-doped carbon nanomaterials have been demonstrated to show excellent electrocatalytic performance for oxygen reduction reaction (ORR) in fuel cells and triiodide reduction in DSSCs.<sup>18-20</sup> While nitrogen-doped carbon nanotubes and nitrogen-doped graphene have been extensively studied, nitrogen-doped graphene nanoribbons have been scarcely reported.<sup>21</sup>

In this paper we report the preparation of nitrogen-doped graphene nanoribbons (N-GNRs) by unzipping carbon nanotubes,<sup>8</sup> followed by thermal annealing under ammonia/argon gas mixture. The resultant N-GNRs showed a high nitrogen content up to 6.5 atom% and a large Brunauer-Emmett-Teller (BET) surface area of 751 cm<sup>2</sup>/g. The use of our N-GNRs as a metal-free counter electrode to replace Pt in DSSCs with T<sub>2</sub>/T<sup>-</sup> electrode led to an energy conversion efficiency even higher than their counterparts with the Pt counter electrode. The observed superior cell performance was attributed to an enhanced charge transfer capability and electrocatalytic activity induced by N-doping.

## Results and discussion

Scheme 1a schematically shows the route to N-GNRs by unzipping carbon nanotubes according to the reported procedure,<sup>8</sup> followed by N-doping via thermal annealing under ammonia/argon gas mixture (see, Experimental Section for details). The resultant N-GNR was then used as a counter electrode in DSSCs with the T<sub>2</sub>/T<sup>-</sup> redox couple electrolyte (Scheme 1b).



**Scheme 1.** Schematic representation of (a) the route to N-doped graphene nanoribbons (*i.e.*, N-GNRs), and (b) Disulfide/thiolate Redox DSSC with the N-GNR as a counter electrode.

Figures 1a & b show scanning electron microscope (SEM) images of the resultant N-GNRs under different magnifications. As can be seen, most of the carbon nanotubes have been unzipped into strip-like graphene. Figure 1c shows the corresponding AFM image, confirming the nanoribbon structure.

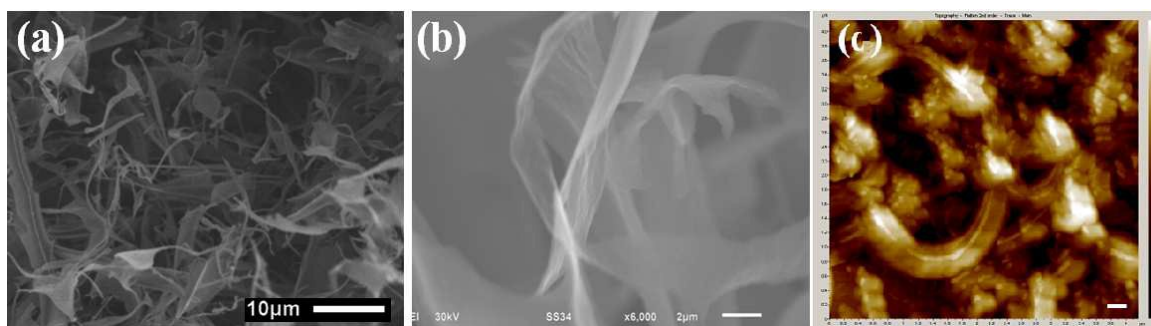


**Figure 1.** (a, b) SEM images of N-GNRs under different magnifications. (c) A typical AFM image of N-GNRs (scale bar: 0.2  $\mu\text{m}$ ).

The nitrogen content of N-GNRs was measured by X-ray photoelectron spectroscopy (XPS). Figure 2a shows a XPS survey spectrum, from which the carbon, nitrogen and oxygen contents were estimated to be 90.4 atom%, 6.5 atom%, 3.1 atom%, respectively. The high resolution XPS

N1s spectrum in Figure 2b shows two component peaks at 398 and 401 eV corresponding to pyridinic nitrogen and graphitic nitrogen, respectively.

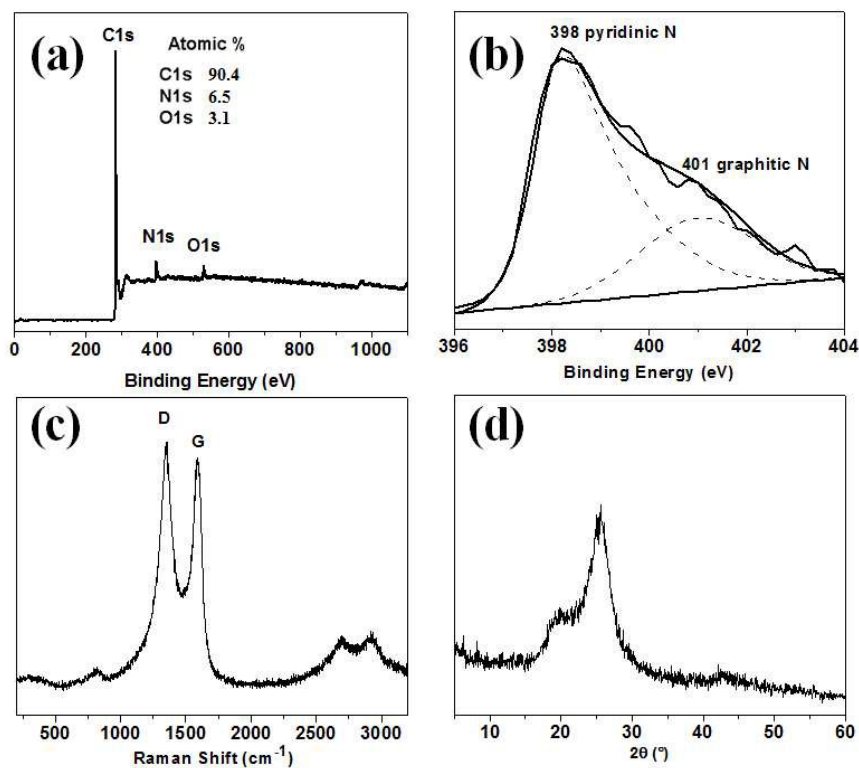


**Figure 2.** (a) XPS spectrum of N-GNR. (b) High-resolution XPS N1s spectrum for N-GNR. (c) Raman and (d) XRD spectra of N-GNR.

Raman spectrum of the N-GNR is given in Figure 2c, which shows a higher D band than the G band with a ratio of  $I_D/I_G = 1.07$ . The observed higher D band than the G band is attributable to the large number of edge and nitrogen-doping induced defects intrinsically associated with the N-GNR, providing an advantage for electrocatalysis. The XRD profile of N-GNR given in Figure 2d shows a peak at about  $2\theta = 26^\circ$  equivalent to the lattice spacing of 0.34 nm corresponding to the (002) facet of graphitic carbon. Nitrogen-doping caused a lattice expansion as evidenced by the appearance of another relatively weak band at  $2\theta = 19^\circ$ , corresponding to an

interlayer distance of 0.47 nm. The surface area was determined by BET measurements (Figure S1) to be as high as  $751 \text{ cm}^2/\text{g}$  for the N-GNR, which is higher than that of a nitrogen-doped graphene<sup>20</sup> or nitrogen-doped carbon nanotubes. The large surface is an additional advantage for electrocatalysis at the counter electrode of a DSSC.

To use the N-GNR as a counter electrode in DSSCs, we transferred it onto a piece of FTO glass. Figure 3a shows a photograph of the N-GNR counter electrode, which is rather uniform and flat. Figure 3b&c reproduce a sideview of the N-GNR counter electrode under different magnifications, showing a foam-like structure. The thickness of the N-GNR counter electrode can be controlled by regulating the conditions for blade coating. Figures 3d&e show the top-view SEM images of the N-GNR counter electrode under different magnifications.

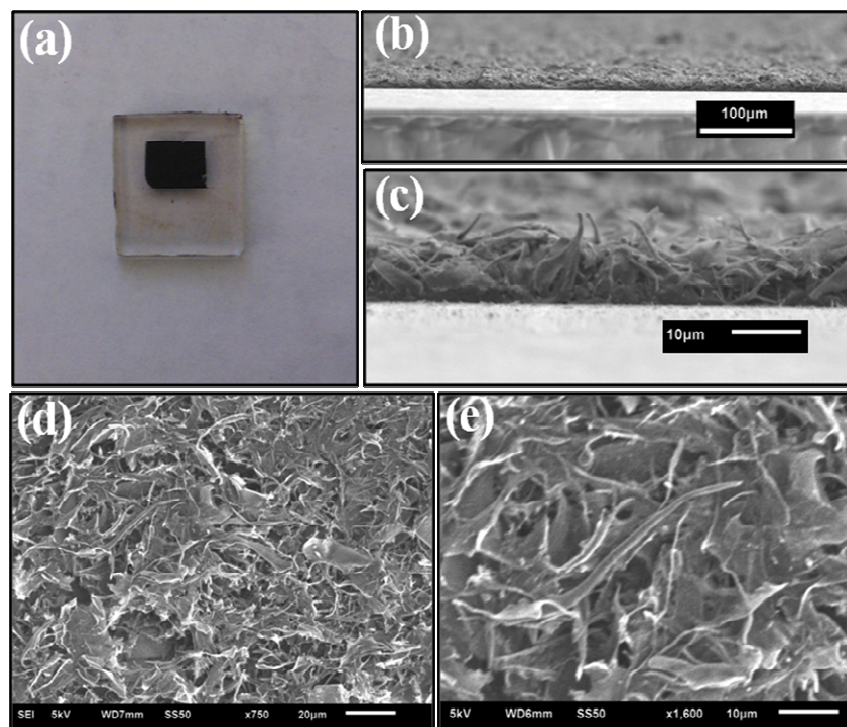


**Figure 3.** (a) Photograph of the N-GNR counter electrode. (b, c) Sideview SEM images and (d, e) top-view SEM images of the N-GNR counter electrode

The N-GNR counter electrode thus prepared was then tested in DSSCs with  $T_2/T^{\cdot-}$  electrolyte.  $T^{\cdot-}$  (*i.e.*, 5-mercapto-1-methyltetrazole ion) and  $T_2$  (*i.e.*, the dimer of  $T^{\cdot-}$ ) were synthesized following the published method and confirmed by NMR (Figure S2).<sup>1</sup> Using the  $T_2/T^{\cdot-}$  redox couple electrolyte, we have prepared several DSSCs with either Pt or N-GNR as the counter electrode. Three N-GNR counter electrodes with the N-GNR foam thickness of 7, 13, and 19  $\mu\text{m}$  (designated as: N-GNRs-1, N-GNRs-2, and N-GNRs-3, respectively) were tested. Figure 4a shows the obtained photocurrent density-voltage (J-V) curves. The corresponding numerical data, including the short circuit current ( $J_{sc}$ ), open circuit voltage ( $V_{oc}$ ), fill factor (FF), and power conversion efficiency (PCE), are listed in Table 1. As can be seen in Table 1, the PCE for DSSCs with the N-GNR counter electrodes are much higher than that of the DSSC with Pt as a counter electrode. The FF for the DSSC with Pt as a counter electrode is only 0.3, which is much lower than those of DSSCs with the N-GNRs as counter electrodes. Furthermore, the short circuit current for DSSCs based on the N-GNR counter electrode increased with increasing the N-GNR thickness, leading to an increased power transfer efficiency (Table 1). The incident photon to charge carrier efficiency (IPCE) for DSSCs with the N-GNRs-3 and Pt counter electrode, respectively, is given in Figure 4b, which, as expected, shows a relatively high IPCE for the DSSC with the N-GNR counter electrode. This is consistent with the electrochemical impedance spectroscopic (EIS) measurements on asymmetric dummy cells with Pt and N-GNRs as the counter electrode, respectively. As seen in Figure 4c, the semicircles of the Nyquist plots for the two N-GNR electrodes are both smaller than that of Pt electrode, indicating smaller charge transfer resistances for the N-GNR electrodes. The charge transfer resistances calculated from the EIS spectra are 12.7, 74.1, and 559.6  $\Omega$  for the NGRs-3, NGRs-1, and Pt electrodes, respectively, showing a strong dependence on the electrode thickness. The series resistances of

the N-GNR counter electrodes are also smaller than that of the Pt counter electrode (Figure 4d).

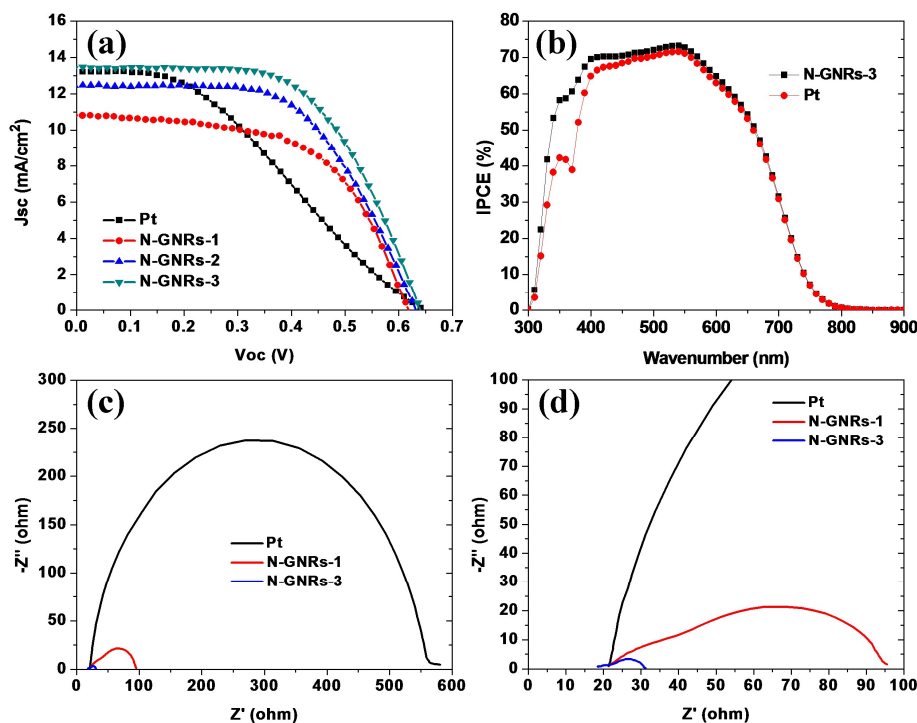


**Figure 4.** (a) Photocurrent density-voltage ( $J - V$ ) curves for DSSCs using  $T_2/T^+$  as the electrolyte redox couple and platinum or N-GNR as the counter electrode. (b) The incident photon to charge carrier efficiency (IPCE) of DSSCs with Pt and N-GNR as the counter electrodes. (c, d) Nyquist plots of asymmetric dummy cells with a Pt and N-GNR counter electrode with different scales.

**Table 1.**  $J_{sc}$ ,  $V_{oc}$ , FF and PCE for DSSCs with the N-GNRs, and Pt as the counter electrode, respectively.

Counter electrode	$J_{sc}$ [mA/cm <sup>2</sup> ]	$V_{oc}$ [V]	FF	PCE [%]
Pt	13.20	0.65	0.36	3.09
N-GNRs-1 (7 $\mu$ m)	10.82	0.62	0.57	3.82
N-GNRs -2 (13 $\mu$ m)	12.47	0.63	0.59	4.64
N-GNRs -3 (19 $\mu$ m)	13.43	0.64	0.59	5.07

In order to investigate the role of nitrogen-doping to the DSSC performance, we also compared the N-GNR counter electrodes with the reduced graphene oxide nanoribbon (rGOR) counter electrode without nitrogen-doping. The photocurrent density-voltage (J-V) curves for DSSCs with the Pt, rGOR, and N-GNR counter electrode (*i.e.*, N-GNRs-3), respectively, are shown in Figure 5a while the corresponding numerical data of the  $J_{sc}$ ,  $V_{oc}$ , FF and PCE are presented in Table 2. As can be seen in Table 2, the PEC of the DSSC with the N-GNRs-3 counter electrode is much higher than that of the DSSC with rGORs as a counter electrode. Furthermore, the resistances of the N-GNR, rGOR and Pt electrodes were also calculated from the EIS measurements on asymmetric dummy cells. The obtained Nyquist plots were given in Figure 5b, which shows a lower charge-transfer resistance and series resistance for the N-GNR counter electrode with respect to the rGOR counter electrode.

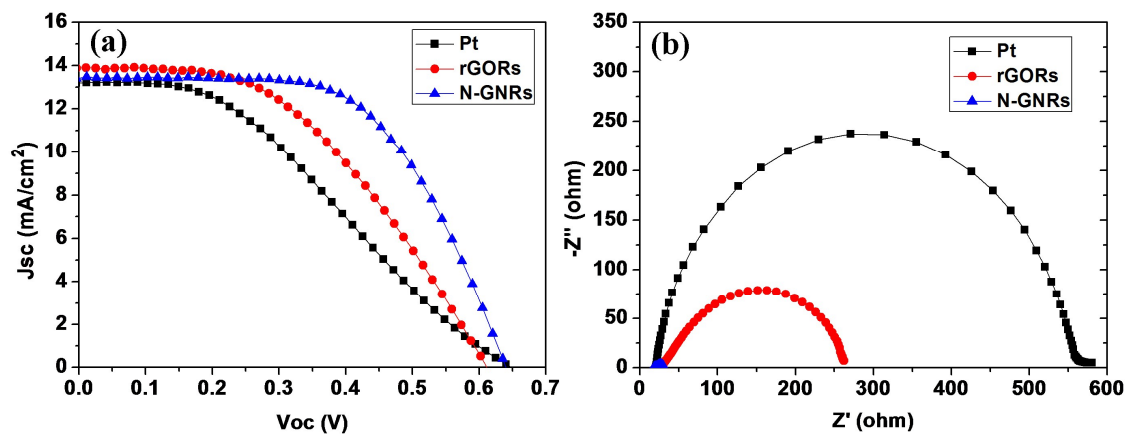


**Figure 5.** (a) Photocurrent density-voltage (J - V) curves for DSSCs using  $T_2/T^-$  as the electrolyte redox couple and platinum, rGORs and N-GNRs-3, respectively, as the counter electrode. (b) Nyquist plots of asymmetric dummy cells with the Pt, rGORs and N-GNRs counter electrode, respectively.

**Table 2.**  $J_{sc}$ ,  $V_{oc}$ , FF and PCE for DSSCs with the Pt, rGOR, and N-GNR as the counter electrode, respectively.

Counter electrode	$J_{sc}$ [mA/cm <sup>2</sup> ]	$V_{oc}$ [V]	Fill Factor	Efficiency [%]
Pt	13.20	0.65	0.36	3.09
rGORs	13.88	0.61	0.46	3.89
N-GNRs-3	13.43	0.64	0.59	5.07

## Conclusions

In summary, we have synthesized nitrogen-doped graphene nanoribbons with a high nitrogen content up to 6.5 atom%. The resultant N-GNR was demonstrated to be efficient counter electrode material, better than platinum, for DSSCs with the disulfide/thiolate ( $T_2/T^-$ ) redox couple electrolyte. Compared with a Pt counter electrode, the N-GNRs counter electrodes possess very low charge transfer resistances. This, together with the large number of the edge/doping-induced defects, makes N-GNRs very efficient counter electrodes for high-performance DSSCs of practical significance.

## Experimental Section

*Preparation of nitrogen-doped graphene nanoribbons.* Graphene oxide nanoribbons were synthesized by chemical unzipping of carbon nanotubes according to the published procedure.<sup>8</sup> The as-prepared graphene oxide nanoribbons in water solution was freeze dried for 3 days to obtain the graphene oxide nanoribbon foam.

Nitrogen-doped graphene nanoribbons were then prepared by annealing the freeze-dried

graphene oxide nanoribbon foams in a quartz tube furnace under ammonia/argon gas mixture. Typically, the graphene oxide nanoribbon foam was firstly placed in a horizontal quartz tube and ammonia/argon gas mixture ( $\text{NH}_3:\text{Ar} = 400 \text{ s.c.c.m.}:400 \text{ s.c.c.m.}$ ) was introduced to the tube. Then, the furnace was heated up from room temperature to  $800 \text{ }^\circ\text{C}$  within 1 hour, and kept at  $800^\circ\text{C}$  for another hour. Thereafter, the quartz tube was air-cooled from the outside to room temperature while keeping the ammonia/argon mixture gas flow rate inside of the quartz tube unchanged. Finally, ammonia was turned off and the sample was taken out from the quartz tube.

*Fabrication of DSSCs:* The N-GNR counter electrode was made by mixing the N-GNR with 5% (wt) PEO solution, which was then coated on the FTO glass and heat treated at  $400 \text{ }^\circ\text{C}$  at air for 3 hours. The Pt counter electrode was prepared by coating Pt catalyst (Pt-Catalyst T/SP, Solaronix) on a FTO glass and calcination at  $400 \text{ }^\circ\text{C}$  for 30 min.

*Preparation of  $\text{TiO}_2$  photoanode:* The FTO glass was cleaned by ultrasonication in scouring agent, isopropanol and ethanol for 10 min, respectively. After drying, FTO was further cleaned by UV- $\text{O}_3$  system at room temperature for 18 min. DSSC was prepared by blade coating  $\text{TiO}_2$  paste (Ti-Nanoxide T, Solaronix) on the freshly cleaned FTO glass substrate using 3M Scotch Magic tape to control the thickness. The  $\text{TiO}_2$  paste was then calcinated at  $450 \text{ }^\circ\text{C}$  for 1 h. The resulting electrode was immersed in a mixture solvent of acetonitrile and isobutanol ( $\text{V}/\text{V}=1/1$ ) solution containing  $0.5 \text{ mM}$  N719 dye (Solaronix) for 24 h to form the sensitized photoanode. Finally, the DSSC cell was fabricated by packaging the photoanode and the counter electrode, and sealed by  $60 \text{ }\mu\text{m}$  thick sealed film (SX1170-60, Solaronix Co) after electrolyte (Iodolyte AN-50 from Solaronix) was added.

## Characterization

X-ray photoelectron spectroscopic (XPS) measurements were carried out on a VG Microtech ESCA 2000 using a monochromic Al X-ray source (97.9 W, 93.9 eV). The Raman spectra were collected using a Raman spectrometer (Renishaw) with a 514 nm laser. The thermogravimetric analysis was performed on a TA instrument with a heating rate of 10 °C. X-ray diffraction (XRD) was measured on a Miniflex II Desktop X-ray diffractometer. Scanning electron microscopic (SEM) images were taken on JEOL JSM-6510LV SEM.

## Acknowledgements

This work was supported financially by AFOSR (FA-9550-12-1-0069), DOD-Army (W911NF-11-1-0209), NSF (CMMI-1400274, IIP-1343270), NSFC-NSF (DMR-1106160), CWRU-WMU (CON115346), NSFC (51202167), and the “Thousand Talents Program” of China.

## References

1. S. Yanagida, Y. H. Yu and K. Manseki, *Acc. Chem. Res.*, 2009, **42**, 1827, and references cited therein.
2. H. J. Snaith and L. Schmidt-Mende, *Adv. Mater.*, 2007, **19**, 3187.
3. T. W. Hamann, R. A. Jensen, A. B. F. Martinson, H. Van Ryswyk and J. T. Hupp, *Energ. Environ. Sci.*, 2008, **1**, 66.
4. M. K. Nazeeruddin, E. Baranoff and M. Gratzel, *Sol. Energy*, 2011, **85**, 1172.
5. B. Oregan and M. Gratzel, *Nature*, 1991, **353**, 737.
6. J. Y. Cong, X. C. Yang, L. Kloo and L. C. Sun, *Energ. Environ. Sci.*, 2012, **5**, 9180.
7. M. K. Wang, N. Chamberland, L. Breau, J. E. Moser, R. Humphry-Baker, B. Marsan, S. M. Zakeeruddin and M. Gratzel, *Nat. Chem.*, 2010, **2**, 385.
8. D. V. Kosynkin, A. L. Higginbotham, A. Sinitskii, J. R. Lomeda, A. Dimiev, B. K. Price and J. M. Tour, *Nature*, 2009, **458**, 872.
9. X. L. Li, X. R. Wang, L. Zhang, S. W. Lee and H. J. Dai, *Science*, 2008, **319**, 1229.

10. D. B. Shinde, J. Debgupta, A. Kushwaha, M. Aslam, V. K. Pillai, *J. Am. Chem. Soc.*, 2011, **133**, 4168.
11. L. Y. Jiao, X. R. Wang, G. Diankov, H. L. Wang and H. J. Dai, *Nat. Nanotechnol.*, 2010, **5**, 321.
12. H. L. Zhang, C. Y. Zhang and D. D. Shi, *Adv. Mater. Res.*, 2011, **148**, 1737.
13. M. Y. Han, B. Ozyilmaz, Y. B. Zhang and P. Kim, *Phys. Rev. Lett.*, 2007, **98**, 206805.
14. L. Tapasztó, G. Dobrik, P. Lambin and L. P. Biro, *Nat. Nanotechnol.*, 2008, **3**, 397.
15. J. Campos-Delgado, J. M. Romo-Herrera, X. T. Jia, D. A. Cullen, H. Muramatsu, Y. A. Kim, T. Hayashi, Z. F. Ren, D. J. Smith, Y. Okuno, T. Ohba, H. Kanoh, K. Kaneko, M. Endo, H. Terrones, M. S. Dresselhaus and M. Terrones, *Nano Lett.*, 2008, **8**, 2773.
16. H. B. Wang, T. Maiyalagan and X. Wang, *ACS Catal.*, 2012, **2**, 781.
17. Y. C. Ma, A. S. Foster, A. V. Krasheninnikov and R. M. Nieminen, *Phys. Rev. B*, 2005, **72**, 205416.
18. K. P. Gong, F. Du, Z. H. Xia, M. Durstock and L. M. Dai, *Science*, 2009, **323**, 760.
19. L. T. Qu, Y. Liu, and J. B. Baek and L. M. Dai, *ACS Nano*, 2010, **4**, 1321.
20. Y. H. Xue, J. Liu, H. Chen, R. G. Wang, D. Q. Li, J. Qu and L. M. Dai, *Angew. Chem. Int. Ed.*, 2012, **51**, 12124.
21. R. Cruz-Silva, A. Morelos-Gomez, S. Vega-Diaz, F. Tristan-Lopez, A. L. Elias, N. Perea-Lopez, H. Muramatsu, T. Hayashi, K. Fujisawa, Y. A. Kim, M. Endo and M. Terrones, *ACS Nano*, 2013, **7**, 2192.